

4

Distributed Acoustic Sensing System Based on Phase-Generated Carrier Demodulation Algorithm

Tuanwei Xu, Shengwen Feng, Fang Li, Lilong Ma, and Kaiheng Yang

ABSTRACT

We demonstrate a real-time distributed acoustic sensing (DAS) system based on phase-sensitive optical time domain reflectometry (Φ -OTDR) and phase-generated carrier (PGC) demodulation algorithm. An unbalanced Michelson interferometer (MI) with specific phase modulation is introduced to overcome phase fading caused by initial phase shift in fiber optic interferometer sensing. Owing to its relatively low data requirement and polarization-independent structure, PGC-DAS system exhibits the superiorities of real-time signal processing and Rayleigh polarization-induced fading suppression. A proof-of-concept system is constructed to demonstrate feasibility and sensing performance. Corresponding to the average phase noise of $\sim 5 \times 10^{-4}$ rad/ $\sqrt{\text{Hz}}$, a strain sensitivity of 8.5 $\mu\epsilon/\sqrt{\text{Hz}}$ is achieved with a spatial resolution of 10 m, as well as a frequency response range of 2 Hz to 1 kHz over 10 km sensing distance. Further, a field trial of this system is presented to validate it in qualitative seismic monitoring on land.

4.1. INTRODUCTION

DAS is an advanced technique developed in recent years to accurately measure ground vibration via fiber optic cables. DAS presents a possible new frontier for recording earthquake waves and other seismic signals in a wide range of research and public safety arenas (Juarez et al., 2005; Parker et al., 2014; Tanimola & Hill, 2009). It repurposes standard telecommunication fiber optic cables as a long series of single-component, in-line strain, or strain-rate sensors, which is a completely differ-

ent way from conventional deployments of nodal devices. DAS can sample passing seismic waves at locations every few meters or closer along paths stretching for tens of kilometers. Therefore, DAS has many advantages, such as passivity, resistance to electromagnetic interference, and cost-effectiveness.

ϕ -OTDR is one of the most widely used schemes to achieve distributed strain or strain-rate sensing. In the early stage, research focused on detecting the interfering Rayleigh backscattering (RB) amplitude in the sensing fiber. In 1993, Taylor and Lee first monitored intrusion events by detecting RB intensity changes with Φ -OTDR technology (Taylor & Lee, 1993). However, the nonlinearity between RB amplitude and vibration could not satisfy the need for quantitative seismic measurement in local and regional seismology. Then, researchers began to investigate phase term (Feng et al., 2018;

Key Laboratories of Transducer Technology, Institute of Semiconductors, Chinese Academy of Sciences, Beijing, China; and

College of Materials Science and Opto-Electronic Technology, University of Chinese Academy of Sciences, Beijing, China

Distributed Acoustic Sensing in Geophysics: Methods and Applications, Geophysical Monograph 268, First Edition.

Edited by Yingping Li, Martin Karrenbach, and Jonathan B. Ajo-Franklin.

© 2022 American Geophysical Union. Published 2022 by John Wiley & Sons, Inc.

DOI:10.1002/9781119521808.ch04

Sha et al., 2017; Yan et al., 2017; Yang et al., 2018; Zinsou et al., 2019), which is almost linear to strain. Currently available DAS systems have characteristics in common that they use pulsed lasers to interrogate optical fibers and process RB phase to provide a nearly continuous estimate of fiber dynamic strain along the fiber. In general, they differ in the method to process RB light and may be separated into coherent detection, dual-pulse detection, and interferometer detection (Hartog, 2017). Coherent detection represents the fact that the phase is extracted by mixing RB signal and local oscillator (He et al., 2017; Lu et al., 2010; Wang et al., 2016). Dual-pulse detection uses two separate RBs with different probe frequencies or phases (Alekseev et al., 2014a, 2014b; Alekseev et al., 2015). Interferometer detection processes RB phase by mixing with itself with a time delay (Masoudi et al., 2013; Wang, Wang, et al., 2015; Wang, Shang, et al., 2015). A coherent heterodyne demodulation DAS system was proposed by Lu et al. (2010). The phase information of heterodyne signal was obtained by mixing the electrical driving signal of acoustic optical modulator (AOM); a spatial resolution of 5 m and a frequency response range of 1 kHz were achieved; and signal-to-noise ratio (SNR) was increased to 6.5 dB with 100 averaging times. To overcome polarization-induced signal fading, an improved polarization-maintaining scheme was presented (Qin et al., 2011). Further, a kind of double-pulse approach was proposed by Alekseev et al. (2014b), which used phase-modulated probe signals with predefined different phase shift sequences of 0 , $-2/3\pi$, and $2/3\pi$. The system demonstrated a distributed phase monitoring capability over 2 km range with 100 Hz sinusoidal strain from piezoceramic modulator. Another dual-pulse DAS system with different frequency shifts was investigated by He et al. (2017). Combined with heterodyne demodulation, the strain frequency response was in the range of 50 Hz to 25 kHz, with a 0.9-73 rad amplitude on a 470 m long optical fiber. There are two kinds of interferometer DAS systems based on 3×3 coupler or PGC demodulation algorithm. For the former, a symmetric 3×3 coupler is adopted to eliminate slow phase shift of the interferometer (Sheem, 1981); the interference phase formed by self-delay of RB in a single pulse is recovered by using the feature of coupler with a phase difference of $\pm 120^\circ$ between output ports. Such an alternative approach was demonstrated by Masoudi et al. (2013); the demonstrated setup has a spatial resolution of 2 m with a frequency range of 500-5000 Hz along 1 km optical fiber (Masoudi et al., 2013). Because of three detectors and a sampling rate of 300 MSa/s per channel, the total data size would reach around 900 MSa/s, which

leads to a huge challenge to realize real-time data processing. For PGC-DAS system (Fang et al., 2015), a PGC was introduced to overcome the initial phase shift problem (Dandridge et al., 1982), and an unbalanced MI with Faraday rotator mirrors (FRMs) was implemented to eliminate the influence of polarization fading (Huang et al., 1996). Compared with 3×3 demodulation, only one detector is needed, and a relatively low data stream helps to online recover phase information.

Here, we present a real-time PGC-DAS system. Combined with characteristics of large dynamic range and high sensitivity of PGC demodulation algorithm (Wang et al., 2015), the proposed system provides an effective technical solution to distributed fiber acoustic sensing. The sensing distance could reach 10 km with the minimum sample interval of 0.4 m. Corresponding to the average phase noise of 5×10^{-4} rad/ $\sqrt{\text{Hz}}$, a strain sensitivity of 8.5 pe/ $\sqrt{\text{Hz}}$ was achieved with a spatial resolution of 10 m, as well as a frequency response range of 2 Hz to 1 kHz over 10 km sensing distance. A field trial of this PGC-DAS system was performed to compare nodal geophones. Results show that seismic records have a high consistency between them, proving the feasibility of PGC-DAS system in seismology.

4.2. PRINCIPLE

The principle of PGC-DAS system is shown in Figure 4.1. A coherent input light pulse passes through a circulator into the sensing optical fiber. RB light enters into an unbalanced MI with FRMs at the ends. There is a phase modulator on one arm of MI and an optical delay L_{MI} on the other arm. RB signal mixes with itself and is detected by one photoelectric detector (PD).

Intensity distribution of RB light is a type of Fourier transform of random permittivity fluctuations (Bao et al., 2016). Assume that the sensing fiber is composed of successive slices with a length of ΔL . Each slice contains M scattering centers, and polarization states between each scattering center are consistent. The interference field of backscattered light at distance $L_m = m\Delta L$ can be expressed by (Park et al., 1998):

$$\begin{aligned} E_{L_m}(t) &= E_0 P_m \exp(-\alpha L_m) \cdot \exp(-j2\beta L_m) \\ &\quad \cdot \sum_{k=1}^M r_k^j \exp(j\phi_k^j) \\ &= E_0 P_m \exp(-\alpha L_m) \cdot \exp(-j2\beta L_m) \cdot a_i \exp[j\phi_i(t)] \end{aligned} \quad (4.1)$$

where E_0 is electric field intensity of the incident light; P_m is polarization-dependent coefficient ranging from 0 to 1; α is optical power attenuation coefficient; r_k and ϕ_k are

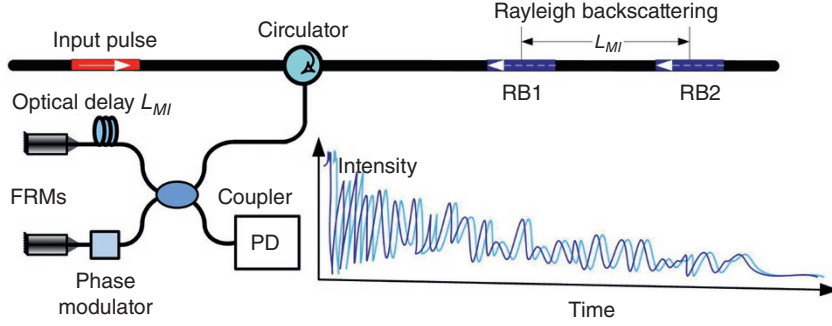


Figure 4.1 Principle of PGC-DAS system with an unbalanced MI.

scattering coefficient and phase of the k th scattering center, respectively; a_i and φ_i are reflectivity and phase of scattering unit, respectively; and β is propagation constant.

Then, scattering light enters into MI, and RB1 and RB2 separated by L_{MI} interference due to the same optical path. The interference electrical field $E(t)$ is written as:

$$\begin{aligned}
 E(t) &= E_L(t) + E_{L-L_{MI}}(t) \\
 &= E_0 P_L a_L \exp(-\alpha L) \cdot \exp(-j2\beta L) \cdot \exp[j\phi_L(t)] \\
 &\quad + E_0 P_{L-L_{MI}} a_{L-L_{MI}} \exp[-\alpha(L-L_{MI})] \\
 &\quad \cdot \exp(-j2\beta L) \cdot \exp[j\phi_L(t)] \\
 &\quad \cdot \exp(j2\beta L_{MI}) \cdot \exp[j\phi_{L-L_{MI}}(t) - j\phi_L(t)] \\
 &= A + B \exp[j\beta L_{MI} + \Delta\phi(t)]
 \end{aligned} \tag{4.2}$$

With simplified coefficients A and B , the interference intensity is given by:

$$\begin{aligned}
 I(t) &= |E(t)|^2 = A^2 + B^2 + 2AB \cos[\beta L_{MI} + \Delta\phi(t)] \\
 &= I_D + I_C \cos[\beta L_{MI} + \Delta\phi(t)]
 \end{aligned} \tag{4.3}$$

For PGC demodulation algorithm, a sinusoidal signal with a modulation frequency of ω_c is loaded on one arm of MI. Therefore, an additional phase modulation $C \cdot \cos(\omega_c t)$ is introduced in Equation 4.3 with $C = m\Delta L_{MI}$, where m is the modulation index and ΔL_{MI} is the maximum length difference variation. Hence, the total phase of the interference light is:

$$\begin{aligned}
 \phi(t) &= C \cdot \cos(\omega_c t) + \beta L_{MI} + \Delta\phi(t) \\
 &= C \cdot \cos(\omega_c t) + \phi(t)
 \end{aligned} \tag{4.4}$$

And the interference intensity is rewritten as:

$$I(t) = I_D + I_C \cos[C \cdot \cos(\omega_c t) + \phi(t)] \tag{4.5}$$

After being multiplied separately with fundamental and second harmonic carriers $\cos(\omega_c t)$ and $\cos(2\omega_c t)$, and later

with low-pass filtering, the in-phase and quadrature components $I_I(t)$ and $I_Q(t)$ are represented as (Dandridge et al., 1982):

$$\begin{aligned}
 I(t) &= -I_c J_1(C) \cdot \sin \phi(t) \\
 Q(t) &= -I_c J_2(C) \cdot \cos \phi(t)
 \end{aligned} \tag{4.6}$$

where $J_1(C)$ and $J_2(C)$ are the first-order and the second-order Bessel function, respectively, of the first kind. When C is equal to 2.63, it satisfies $J_1(C) = J_2(C)$. Thus, the phase $\phi(t)$ is calculated by:

$$\phi(t) = \arctan[I(t)/Q(t)]. \tag{4.7}$$

4.3. EXPERIMENTS AND RESULTS

The PGC-DAS system setup is illustrated in Figure 4.2. A 1550.15 nm coherent laser with a bandwidth of 3 kHz is modulated by AOM with an extinction ratio of 50 dB to an optical pulse. The pulse width and repetition rate are 50 ns and 8 kHz, respectively. The pulse light travels through an optical isolator (ISO) and is amplified by an erbium-doped fiber amplifier (EDFA). A fiber Bragg grating is utilized to filter redundancy in amplified spontaneous emission (ASE). The filtered pulse light is launched into the sensing fiber through a circulator. After that, RB light is injected into an unbalanced MI with a one-way optical path difference of 10 m, i.e., $L_{MI} = 10$ m. FRMs are used to eliminate the influence of polarization fading. The mixed interference RB light is modulated by a sinusoidal signal with a modulation amplitude of 2.63 rad and arrives at the high-sensitivity optical detector (PD) with a bandwidth of 80 MHz. After analog-to-digital conversion at the analog digital converter (ADC), the obtained RB signal is sampled with a sampling rate of 250 MS/s, corresponding to the minimum sampling interval of 0.4 m. PGC demodulation scheme is implemented on a digital processing unit consisting of field programmable gate array/digital signal processor (FPGA/DSP)

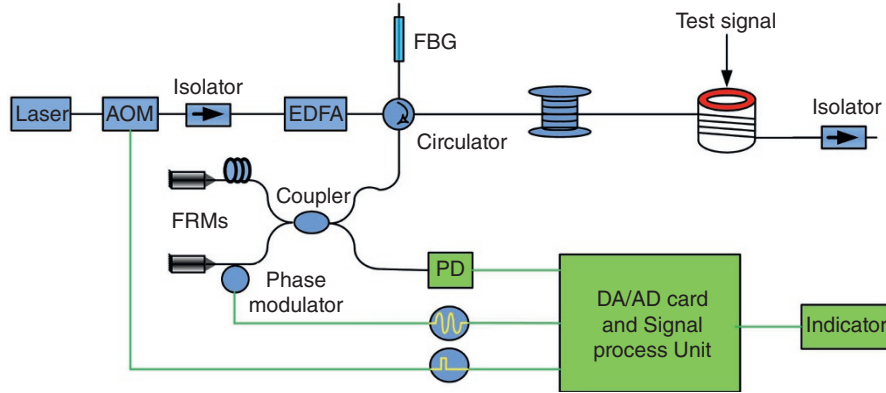


Figure 4.2 Setup of PGC-DAS system.

circuits and a real-time controller, which could realize more than 10,000 channels’ real-time phase calculation. The sensing fiber is a 10 km standard single-mode fiber, and a fiber stretcher with a 6 m single-mode fiber wound on a piezoelectric ceramic tube is inserted in the sensing fiber as a unit under test. An isolator is placed at the end of the sensing fiber to remove unwanted end reflection.

The time series in Figure 4.3a contains 9,995 data points of Channel #4750. These data points are sampled with a time increment of 0.5 ms, which conceivably allows the time series to contain frequency content up to a Nyquist frequency of 1 kHz (Figure 4.3b). To remove quasi-static phase drift caused by environmental effects, a high-pass filter with a cutoff frequency of 2 Hz is adopted in the procedure. Thus, the frequency response range is limited to 2 Hz to 1 kHz.

Under the equation $\delta\varepsilon = \delta\varphi/(2\pi nL_{MI}/\lambda)$, the strain sensitivity is mainly determined by the phase noise $\delta\varphi$ and the spatial resolution L_{MI} (defined as the gauge length [Masoudi et al., 2013]). The phase noise is shown in Figure 4.3b, and the average value is around $5 \times 10^{-4} \text{rad}/\sqrt{\text{Hz}}$. With the designed spatial resolution $L_{MI} = 10 \text{ m}$, the minimum detected strain of this PGC-DAS system is as small as $8.5 \text{ }\mu\text{e}/\sqrt{\text{Hz}}$.

Figure 4.4a displays a waterfall plot of the magnitude response of each channel in the sensing fiber around the fiber stretcher with a sinusoidal signal of 100 Hz. The y-axis is proportional to distance along the cable, with a distance increment of 0.4 m, and the color of each cell is proportional to the waveform amplitude. Figure 4.4b shows the superposition result of absolute amplitude of each channel. The signal boundary is defined by the channel of 10% of the absolute peak amplitude. Results show

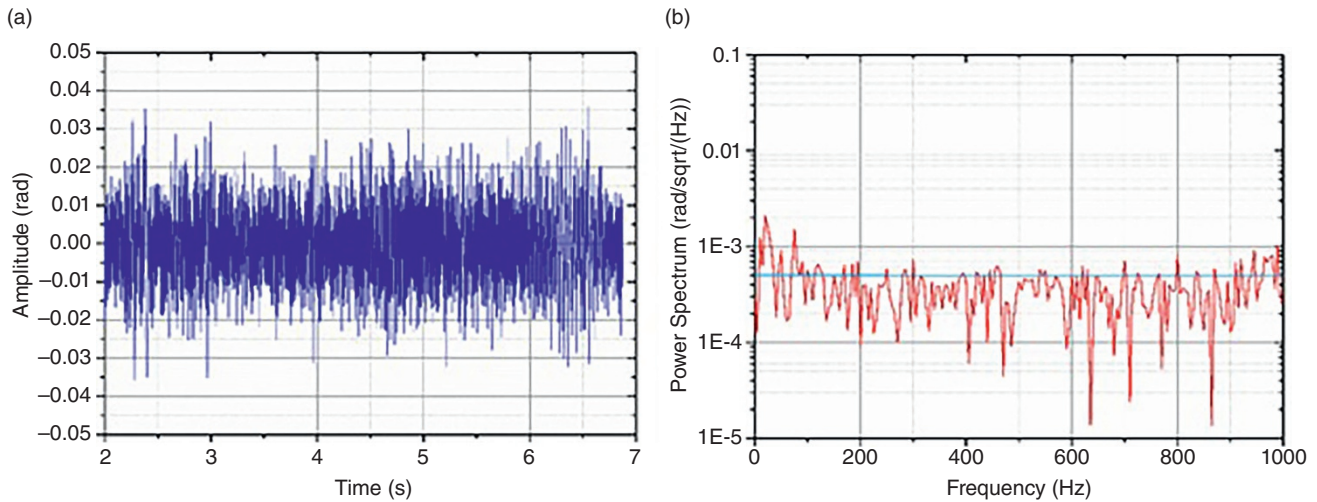


Figure 4.3 Phase noise of PGC-DAS system on Channel #4750: (a) Time series and (b) power spectrum.

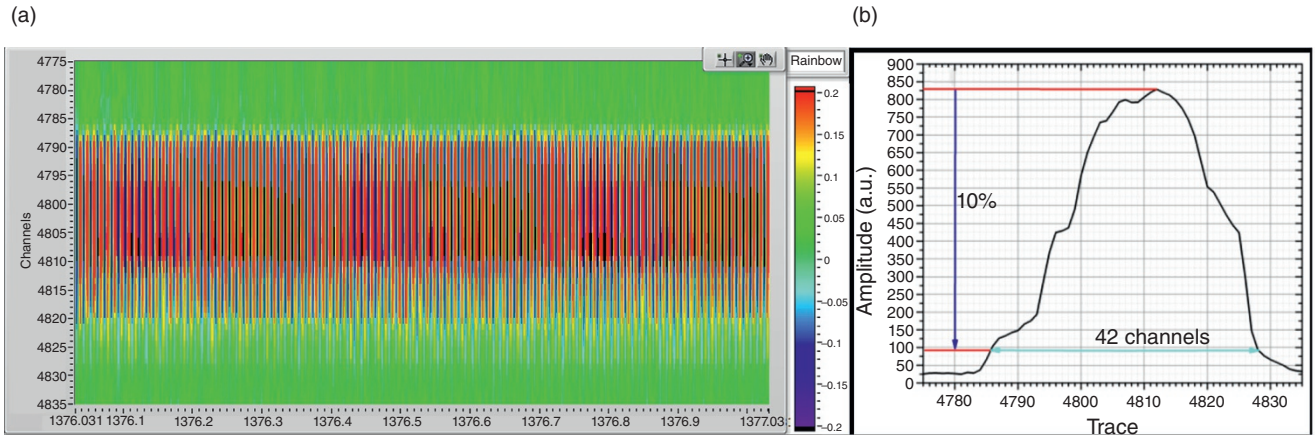


Figure 4.4 Intensity map of demodulation magnitude of each channel: (a) Waterfall plot and (b) superposition absolute magnitude.

that the sinusoidal signal ranges from Channel #4786 to Channel #4828, and the range is up to 16.8 m. By subtracting the coiled fiber length, the spatial resolution of PGC-DAS system is about 10.8 m, which is nearly consistent with the optical path difference $L_{MI} = 10$ m.

Figure 4.5 depicts the measurement of frequency response with a linear sweeping frequency signal from 2 Hz to 1 kHz. Each sweeping signal with a constant voltage amplitude of 0.5 Vpp lasts 2 s. Short-time Fourier transform (STFT) is used to indicate the relative linear and flat frequency response of PGC-DAS system.

The linearity of PGC-DAS system is an essential characteristic of quantitative seismic measurement. A sinusoidal strain signal of the fiber stretcher with sweeping voltage from 0.01 Vpp to 1.6 Vpp is used to inspect the amplitude response. The linearity of the strain response is shown in Figure 4.6. From the fitting result, the linear coefficient R^2 is 0.99941. An expected linear response capability is presented, and it proves the feasibility of the PGC-DAS system for the microseismic signal detection.

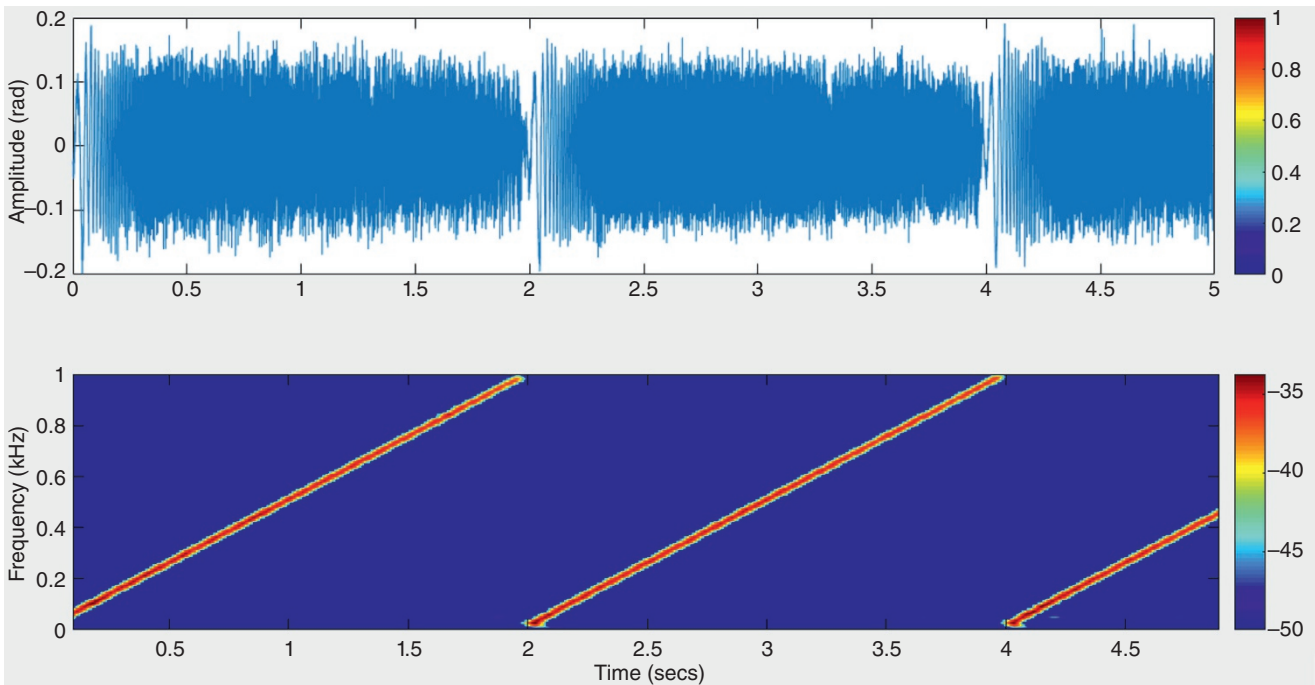


Figure 4.5 Time domain and STFT spectrogram of sweeping frequency signal.

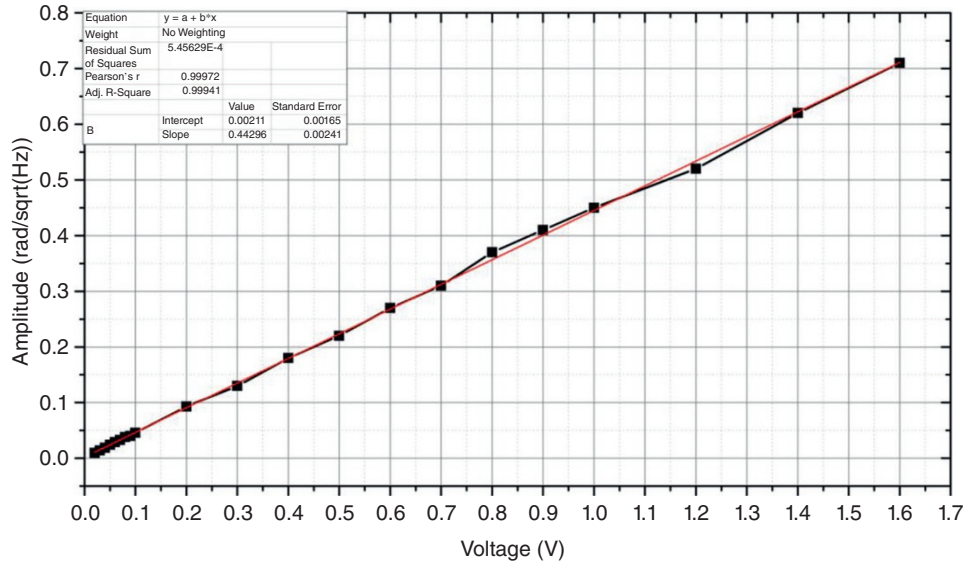


Figure 4.6 Amplitude response curve of PGC-DAS system.

4.4. FIELD TRIAL OF NEAR-SURFACE SEISMIC EXPERIMENT WITH PGC-DAS SYSTEM

A near-surface seismic experiment based on fiber optic cables and PGC-DAS system was conducted in Hebei Province, China. On the site, a 7 mm diameter fiber optic cable (Figure 4.7d) of about 430 m was buried in an approximate L shape at 0.4 m depth with a 230 m cable in Line 1 and a 200 m cable in Line 2 (Figures 4.7a and 4.7b). PGC-DAS system was connected at one end of the fiber optic cable to record multichannel seismic data at a sampling rate of 2 kHz with a spatial sampling interval of 1 m. For comparison, 80 conventional three-component (3C) geophones (Figure 4.7c) were buried along the cable with an interval of around 5 m. A vibroseis truck was employed as an active source at seven designed positions (P1, P2, P3, P4, P5, P6, and P7) around the fiber optic cable to investigate directivity, since optical fiber is mostly sensitive to axial strain along the fiber and lacks broadside sensitivity due to its silica glass nature.

Figure 4.8 shows multichannel seismic recordings of PGC-DAS system and geophone array in Line 1 at active source position #1. Since axial is the most sensitive direction of the fiber, the data of a 3C geophone for x -component were used. Both 40 channels' recordings for DAS system and geophones' array with the same interval of 5 m at similar positions were selected. Difference of seismic first arrivals' time between those two systems is due to trigger unsynchronization. DAS data were qualitatively similar to the signals observed on the geophones. Both direct wave and surface were clearly presented.

However, there was apparently isolated noise in DAS data before the first arrivals (e.g., in Channels of 11, 151, and 161) due to interference fading. Simple contrast shows that this PGC-DAS system can provide reliable information to image and explore the shallow subsurface under this fiber cable.

4.5. CONCLUSIONS

We propose a real-time DAS system based on PGC demodulation algorithm. Compared with the previous work (Fang et al., 2015), it brings a 15.6 dB improvement in phase noise. The average noise could reach $\sim 5 \times 10^{-4}$ rad/ $\sqrt{\text{Hz}}$, and the strain sensitivity is as small as 8.5 $\mu\text{e}/\sqrt{\text{Hz}}$ for a 10 m spatial resolution. This PGC-DAS system could measure the dynamic vibration signal from 2 Hz to 1 kHz over a 10 km long optical fiber, with a linear coefficient R^2 of 0.99941 and a minimum spatial interval of 0.4 m. The near-surface seismic experimental results show that DAS data are qualitatively similar to the signals observed on the geophones. These facts suggest that DAS technology provides a novel and highly valuable tool for geophysical science in a wider sense. Moreover, PGC-DAS system has potential advantages in reducing size and power consumption due to simple structure and efficient phase demodulation algorithm, and a mini-PGC-DAS module is under development, with a size of 150 mm \times 300 mm \times 110 mm (width \times depth \times height) and a power consumption of 25 W, which could work at the bottom for submarine application.



Figure 4.7 Field trial of near-surface seismic experiment. (a) Plan view of experimental layout, (b) photo of the buried fiber optic cable, (c) photo of a 3C geophone, and (d) structure of the fiber optic cable.

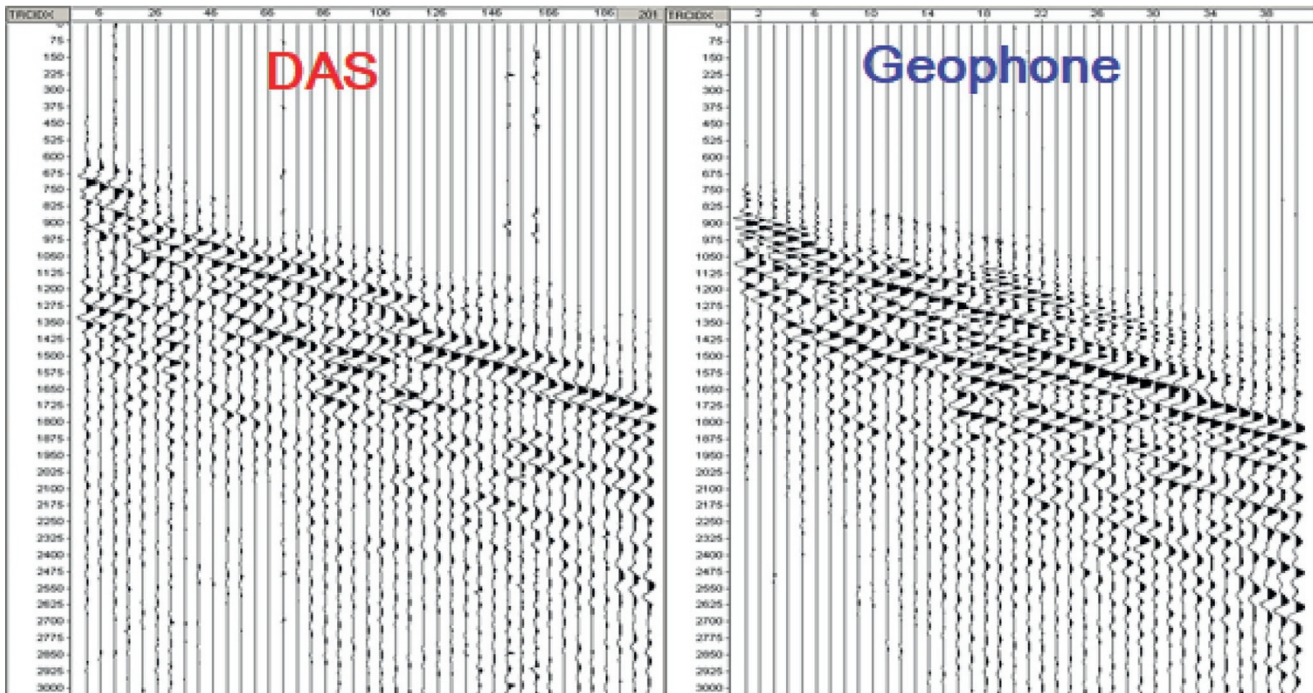


Figure 4.8 Initial data of DAS system and geophone array for x-component at P1 in Line 1.

ACKNOWLEDGMENTS

This work was funded by the National Natural Science Foundation of China (Grant Nos. 61875184 and 61775210), the National Key Research and Development Program of China (Grant No. 2017YFB0405500), the Strategic Priority Research Program of the Chinese Academy of Sciences (Grant Nos. XDC02040500 and XDA22040105), and State Key Laboratory of Geodesy and Earth's Dynamics, Institute of Geodesy and Geophysics, Chinese Academy of Sciences (Grant No. SKLGED2019-5-4-E).

REFERENCES

- Alekseev, A. E., Vdovenko, V. S., Gorshkov, B. G., Potapov, V. T., & Sergachev, I. A. (2014a). A phase-sensitive optical time-domain reflectometer with dual-pulse phase modulated probe signal. *Laser Physics*, 24(5).
- Alekseev, A. E., Vdovenko, V. S., Gorshkov, B. G., Potapov, V. T., & Sergachev, I. A. (2014b). Phase-sensitive optical coherence reflectometer with differential phase-shift keying of probe pulses. *Quantum Electronics*, 44(10), 965–969.
- Alekseev, A. E., Vdovenko, V. S., Gorshkov, B. G., Potapov, V. T., & Simikin, D. E. (2015). A phase-sensitive optical time-domain reflectometer with dual-pulse diverse frequency probe signal. *Laser Physics*, 25(6), 065101.
- Bao, X., Zhou, D., Baker, C., & Chen L. (2017). Recent development in the distributed fiber optic acoustic and ultrasonic detection. *Journal of Lightwave Technology*, 35(16), 3256–3267.
- Dandridge, A., Tveten, A. B., & Giallorenzi, T. G. (1982). Homodyne demodulation scheme for fiber optic sensors using phase generated carrier. *IEEE Journal of Quantum Electronics*, 18(10), 1647–1653.
- Fang, G., Xu, T. W., Feng, S. W., & Li, F. (2015). Phase-sensitive optical time domain reflectometer based on phase generated carrier algorithm. *Journal of Lightwave Technology*, 33(13), 2811–2816.
- Feng, S., Xu, T., Huang, J., Yang, Y., Ma, L., & Li, F. (2018). Sub-meter spatial resolution phase-sensitive optical time-domain reflectometry system using double interferometers. *Applied Sciences*, 8(10), 1899.
- Hartog, A. (2017). *An introduction to distributed optical fiber sensors*. CRC Press, Taylor & Francis Group.
- He, X., Liu, F., Qin, M., Cao, S., Gu, L., Zheng, X., & Zhang, M. (2017). Phase-sensitive optical time-domain reflectometry with heterodyne demodulation. 2017 25th Optical Fiber Sensors Conference (OFS) (pp. 1–4).
- Huang, S., Lin, W., Chen M., Hung, S., & Chao, H. (1996). Crosstalk analysis and system design of time-division multiplexing of polarization-insensitive fiber optic Michelson interferometric sensors. *Journal of Lightwave Technology*, 14(6), 1488–1500.
- Juarez, J. C., Maier, E. W., Choi, K. N., & Taylor, H. F. (2005). Distributed fiber-optic intrusion sensor system. *Journal of Lightwave Technology*, 23(6), 2081–2087.
- Lu, Y., Zhu, T., Chen, L., & Bao, X. (2010). Distributed vibration sensor based on coherent detection of phase-OTDR. *Journal of Lightwave Technology*, 28(22), 3243–3249.
- Masoudi, A., Belal, M., & Newson, T. P. (2013). A distributed optical fibre dynamic strain sensor based on phase-OTDR. *Measurement Science and Technology*, 24(8), 085204.
- Park, J., Lee, W., & Taylor, H. F. (1998). *Fiber optic intrusion sensor with the configuration of an optical time-domain reflectometer using coherent interference of Rayleigh backscattering*. Proceedings of SPIE 3555, Optical and Fiber Optic Sensor Systems.
- Parker, T., Shatalin, S., Farhadiroushan, M., Kamil, Y., Gillies, A., Finfer, D., & Estathopoulos, G. (2012). *Distributed Acoustic Sensing—a new tool for seismic applications*. 74th EAGE Conference & Exhibition incorporating SPE EUROPEC 2012.
- Qin, Z., Zhu, T., Chen, L., & Bao, X. (2011). High sensitivity distributed vibration sensor based on polarization-maintaining configurations of phase-OTDR. *IEEE Photonics Technology Letters*, 23(15), 1091–1093.
- Sha, Z., Feng, H., & Zeng, Z. (2017). Phase demodulation method in phase-sensitive OTDR without coherent detection. *Optics Express*, 25(5), 4831–4844.
- Sheem, S. K. (1981). Optical fiber interferometers with [3x3] directional-couplers—analysis. *Journal of Applied Physics*, 52(6), 3865–3872.
- Tanimola, F., & Hill, D. (2009). Distributed fibre optic sensors for pipeline protection. *Journal of Natural Gas Science and Engineering*, 1(4), 134–143.
- Taylor, H. F., & Lee, C. E. (1993). Apparatus and method for fiber optic intrusion sensing. Patent US5194847 A.
- Wang, C., Shang, Y., Liu, X. H., Wang, C., Yu, H. H., Jiang, D. S., & Peng, G. D. (2015). Distributed OTDR-interferometric sensing network with identical ultra-weak fiber Bragg gratings. *Optics Express*, 23(22), 29038–29046.
- Wang, C., Wang, C., Shang, Y., Liu, X., & Peng, G. (2015). Distributed acoustic mapping based on interferometry of phase optical time-domain reflectometry. *Optics Communications*, 346, 172–177.
- Wang, Z. N., Zhang, L., Wang, S., Xue, N. T., Peng, F., Fan, M. Q., et al. (2016). Coherent Phi-OTDR based on I/Q demodulation and homodyne detection. *Optics Express*, 24(2), 853–858.
- Yang, G., Fan, X., Liu, Q., & He, Z. (2018). Frequency response enhancement of direct-detection phase-sensitive OTDR by using frequency division multiplexing. *Journal of Lightwave Technology*, 36(4), 1197–1203.
- Yan, Q., Tian, M., Li, X., Yang, Q., & Xu, Y. (2017). *Coherent Phi-OTDR based on polarization-diversity integrated coherent receiver and heterodyne detection*. 2017 25th Optical Fiber Sensors Conference (OFS) (pp. 1–4).
- Zinsou, R., Liu, X., Wang, Y., Zhang, J., & Wang, Y. (2019). Recent progress in the performance enhancement of phase-sensitive OTDR vibration sensing systems. *Sensors (Basel)*, 19(7), 1709.